COMPDYN 2013
4th ECCOMAS Thematic Conference on
Computational Methods in Structural Dynamics and Earthquake Engineering
M. Papadrakakis, V. Papadopoulos, V. Plevris (eds.)
Kos Island, Greece, 12–14 June 2013

# CHARACTERISATION OF THE AERODYNAMIC BEHAVIOUR OF THE GRANDE RAVINE VIADUCT FROM PROTOTYPE MONITORING

**Fernando Bastos[1], Elsa Caetano[1], Álvaro Cunha[1], Xavier Cespedes[2], Mathieu Arquier[2], Olivier Flamand[3]**

[1] ViBest, Faculty of Engineering, University of Porto
R. Dr. Roberto Frias, 4200-465 Porto, Portugal
ecaetano@fe.up.pt

[2] SETEC Tpi
Paris 42/52, quai de la Rapée, 7, 75 583 Paris cedex12
cespedes@tpi.setec.fr

[3]Centre Scientifique et Technique du Bâtiment
11 rue Henri Picherit- 44300 Nantes- France
olivier.flamand@cstm.fr

**Keywords:** Wind monitoring; Full-scale measurements; Bridge Aerodynamics.

**Abstract.** *The Grande Ravine Viaduct, at the Reunion Island, is a girder bridge crossing an abrupt volcanic breach conceived and designed by Alain Spielmann and the design office SETEC TPI [1]. The location in a zone frequently affected by typhoons and the typology of the bridge, for which limited experience existed previously in terms of description of the wind behaviour, motivated the installation of a monitoring system, in order to characterise the wind loads acting on the bridge, the corresponding aerodynamic behaviour and the structure dynamic response. The monitoring system comprehends various anemometers distributed along and outside the bridge, pressure and temperature sensors and accelerometers.*

*In the context of a collaboration established between the Designer, ViBest/FEUP and CSTB, the data recorded by the monitoring system for a period of 3 years has been analysed, allowing the comparison between the characteristics of the wind model based on site measurements and the wind parameters defined at design stage based on numerical computational fluid dynamics and wind tunnel tests studies.*

*In this context, it is the purpose of this paper to present and discuss preliminary results of the prototype monitoring during a 2-year period, describing in particular numerical tools implemented with the purpose of selecting relevant data, processing signals and extracting relevant effects in terms of the wind response.*

## 1 INTRODUCTION

Crossing an abrupt breach 320 m in width and 170 m in depth, the Grande Ravine Viaduct, at the Reunion Island, is a girder bridge with a total length of 288 m (Figure 1) located in a zone frequently affected by typhoons.

The characteristics of this structure [1], which lead to a classification as stiff when compared to well studied cable-stayed and suspension bridges, although flexible when compared with typical girder bridges, point to a limited experience in terms of the aerodynamic characterisation. In particular, some hypotheses required by the typical wind tunnel tests of physical models, by the numerical computational fluid dynamic studies and by the wind formulations of the structural response require validation.

At the same time, the availability at the present moment of robust technology for full scale monitoring of structures, combined with the evolution in data communication, which allow the storage and remote transfer of significant volumes of data, suggest the characterisation of local wind by means of "in situ" monitoring, based on an adequate spatial distribution of anemometers in order to validate and improve consolidated design methodologies, and permit also the monitoring of the response for establishment of correlations with the wind loads.

Having these aspects into consideration, SETEC promoted the installation of an aerodynamic monitoring system on the bridge [2]. This system comprehends various anemometers, pressure and temperature sensors and accelerometers, and has been operating for a period of 3 years. Collaboration with ViBest/ FEUP and with CSTB has been established, with the purpose of processing and interpreting the prototype data and validating design hypotheses and studies.

This paper presents and discusses preliminary results of the prototype monitoring based on the data collected during a 2-year period. Some aspects of the management of the huge database and of the tools implemented with the purpose of selecting relevant data, processing signals and extracting relevant effects in terms of the wind response are described.

Figure 1: Grande Ravine viaduct, site image.

## 2 BRIDGE CHARACTERISTICS AND MONITORING SYSTEM

The Grande Ravine viaduct is a motorway bridge formed by a steel orthotropic deck 22.7 m in width and 4 m in height continuous over the 288 m length (Figure 2). The deck is supported by inclined cantilevered struts made of high resistance concrete, at angles of 20° to the horizontal, fitted in a counter balancing concrete abutment founded in solid rock.

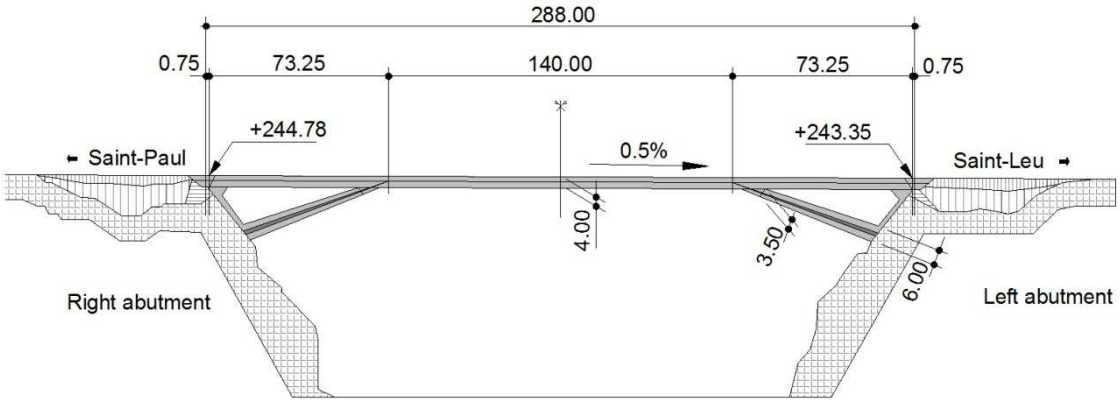


Figure 2: Profile of the Grande Ravine Viaduct.

The monitoring system installed by ADVITAM [3], whose instrumentation layout is represented in Figure 3, comprehends the following devices: 4 sonic anemometers, distributed along the bridge and mounted on 3.5 m high masts; one propeller anemometer, mounted on a 10 m high mast positioned outside the viaduct at a distance of 250 m from one of the abutments; 14 pressure transducers, distributed in two sections close to the mid-span; external temperature sensors coupled with the anemometers, and internal temperature sensors placed in the same cross sections of the pressure sensors; and 6 accelerometers mounted in vertical and transversal direction in three sections along the deck.

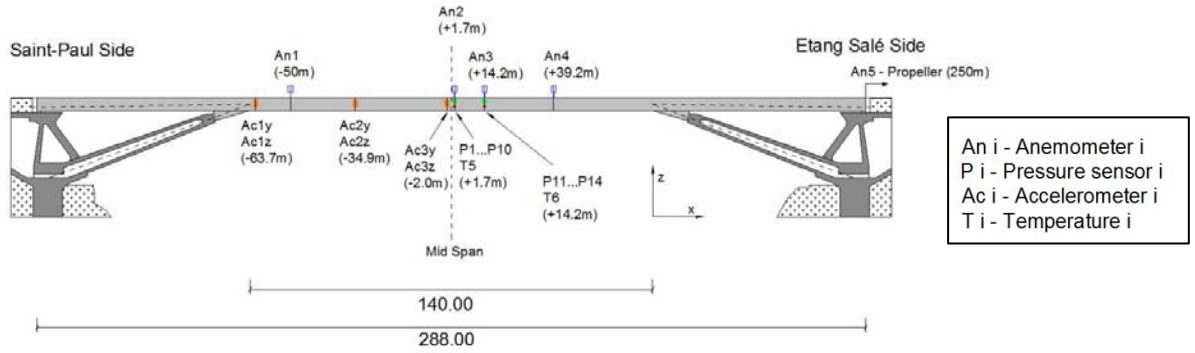


a)

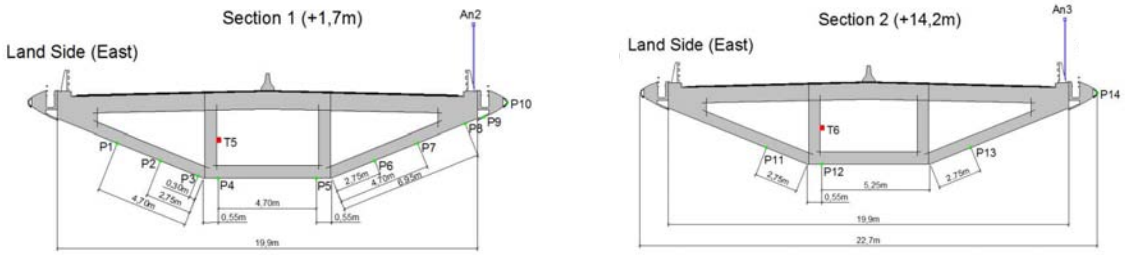


c)

Figure 3: Layout of instrumentation: (a) distribution of sensors along the viaduct profile; (b) pressure sensors in section 1, +1,7m from mid-span; (c) pressure sensors in section 2, +14,2m from mid-span.

The acquisition system is based on a MOXA card, that groups the signals from the sonic anemometers, and on a 16-bit National Instruments acquisition card that digitises the signals from the accelerometers, temperature and pressure sensors. The propeller anemometer signals are conditioned by a ICP converter connected by serial port to the acquisition computer. Data acquisition is made by a software developed by ADVITAM [3] in the LABVIEW platform and has been programmed to sample for continuous periods of 13 minutes using different sampling frequencies for the different sensors: sonic and propeller anemometers are sampled at 32Hz and 5Hz, respectively; accelerometers are sampled at 1000Hz; pressure sensors, at 300Hz, and temperature sensors, at 10Hz. Implemented in the acquisition software is a routine to filter, re-sample at 40Hz and record data into text files. Each file stores 32321 lines of the 40 channel data (14 from the anemometers, 14 from the pressure sensors, 6 from temperature sensors and 6 from the accelerometers). Text records are saved in a computer located inside the bridge deck and then transferred to a computer in FEUP by a management routine that comprises the download via FTP, storage and backup of files.

The monitoring system has been operating continuously since December 2009, with occasional interruptions due to power failure and maintenance activities.

The raw data stored in the computer at FEUP are processed by a code developed in the MATLAB platform. This code was developed aiming at: characterising the wind model in the Grande Ravine bridge site; characterising the bridge behaviour in operational conditions; and, particularly, characterising the structural behaviour under the local wind excitation.

The methodology adopted in the development of this code follows the diagram presented in Figure 4. The Preliminary Processing routine comprehends an initial check of data by inspecting the text files for irregular situation, detecting for example, breaks in acquisition, correcting and packing valid records into MATLAB binary format files (.mat). Subsequently, the signals are re-sampled, de-spiked and finally decimated to 20Hz.

The Global Processing routine provides a global statistic analysis of the records. Mean, maximum, standard-deviation estimates are computed for all signal sensors. Wind records are processed in order to characterise the global atmospheric pattern and the acceleration records are treated with the objective of identification of the dynamic structural properties (natural frequencies, modal configurations and modal damping).

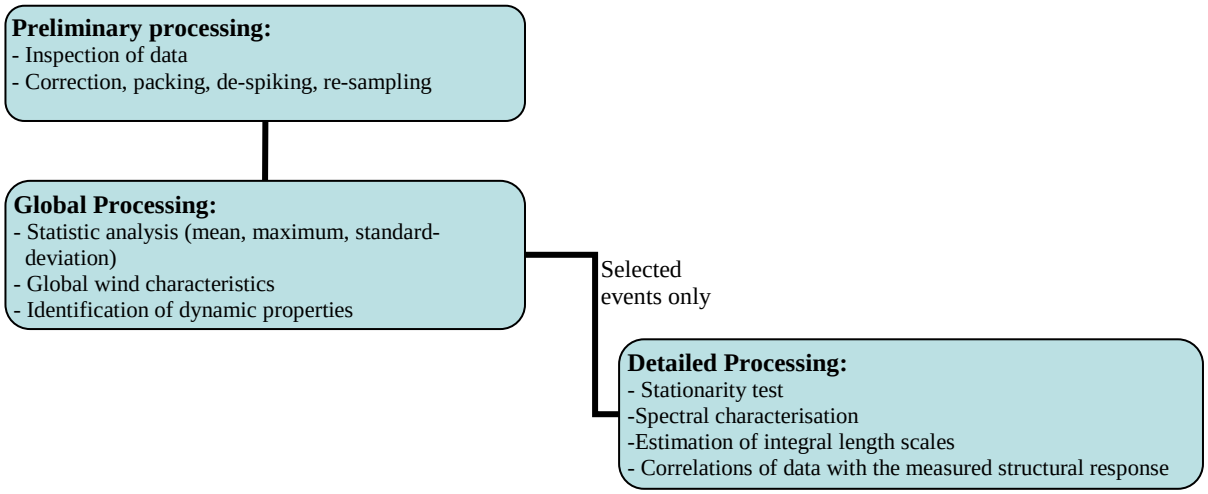


Figure 4: Methodology for data processing.

The Detailed Processing routine is applied only to selected events, for example to the records exceeding some wind velocity threshold. The wind data is sorted by 10-minute mean

wind events higher than a defined threshold and subjected to a stationarity test. The detailed processing of wind records comprehends a spectral characterisation, with estimation of correlation and integral length scales. Correlations of these quantities with pressure data and with the structural response captured by the accelerometers are then established.

## 3 ANALYSIS OF FULL-SCALE DATA

The diversity of the sensors integrating the monitoring system demands different, although articulated strategies in the processing of data. These respect specifically the wind records, the pressure and the acceleration measurements. The following sections will focus only on the wind data analysis.

The results presented in this section respect a period of 24 months, from January 1st to 31st December 2012.

The wind signals are acquired in the anemometer referential, in the form of a horizontal direction, a horizontal velocity and vertical velocity. After packaging and preliminary processing, the data are transformed into the referential of mean wind velocity and treated on the basis of 10-minute intervals.

The global analysis of mean velocity data during the studied period, shows that the 10-minute mean wind velocity is quite low (Figure 5a)), of the order of 2.5 m/s, reaching in very few situations mean velocities above 11 m/s (Figure 5b)). Despite the location in an area of high cyclonic risk, in the period under analysis no significant event of such nature occurred.

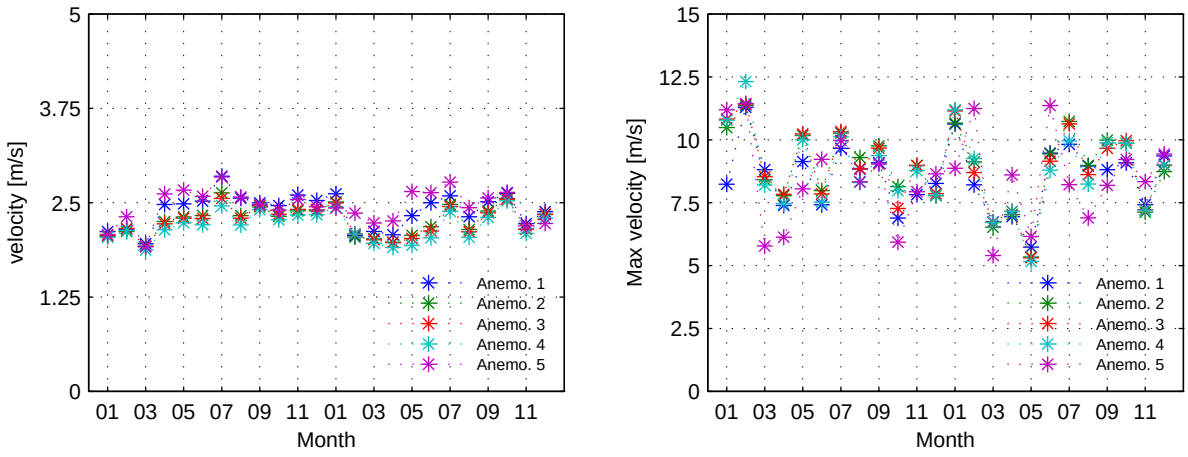


a) b)

Figure 5: (a) Monthly averaged 10-minute mean wind velocity and (b) monthly maximum 10-minute mean wind velocity.

For detailed processing, only time series with 10-minute mean velocity higher than 5m/s were selected. The time series satisfying this criterion were further screened through stationarity tests. From the two-year period in analysis, it was concluded that only about 3% of the records have 10-minute mean velocity exceeding 5m/s and less than 2.45% of the data exhibit stationary properties [4].

In order to understand particular characteristics of the wind at the bridge site, the ratio between the mean velocity recorded by each of the sonic anemometers U and the reference propeller anemometers $U_{prop}$ has been calculated and is represented in the "rose" of Figure 6a). This figure evidences higher values of $U/U_{prop}$ for directions [50,135] and [200,315], which coincide with the ravine and are almost perpendicular to the viaduct, whose axis is marked by the line in the rose representation. Figure 6b) shows also that $U/U_{prop}$ grows with the mean

wind velocity. It is concluded that the wind aligned with the ravine is higher than the reference propeller velocity.

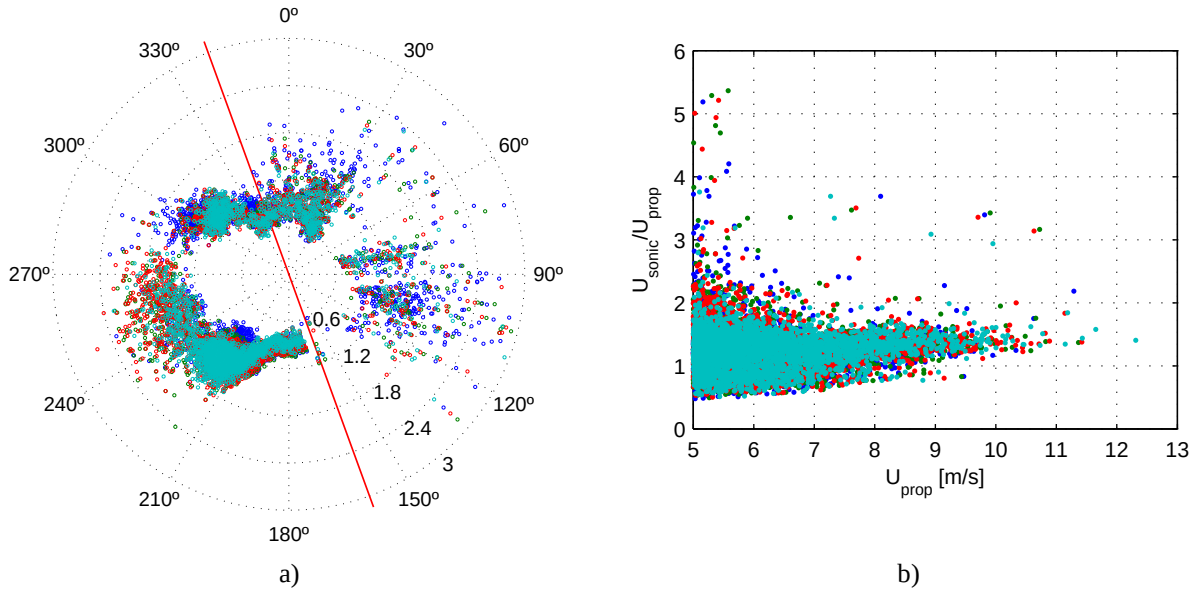


a) b)

Figure 6: Ratio $U/U_{prop}$ as function of direction (a) and reference velocity (b).

Another aspect to analyse refers to the understanding of how the presence of a ravine with very abrupt walls influences the wind along the bridge.

A comparison of synchronous directions registered by the sonic anemometers with the reference propeller can be observed in Figure 7. The analysis of this figure evidences generally a linear relationship between site and reference propeller directions. Exception is made to the direction intervals [60,150] and [215,285] in which sonic anemometers register a quasi constant direction defined in the ranges [85,105] and [260,275], respectively. These constant directions reflect the alignment of the wind with the ravine.

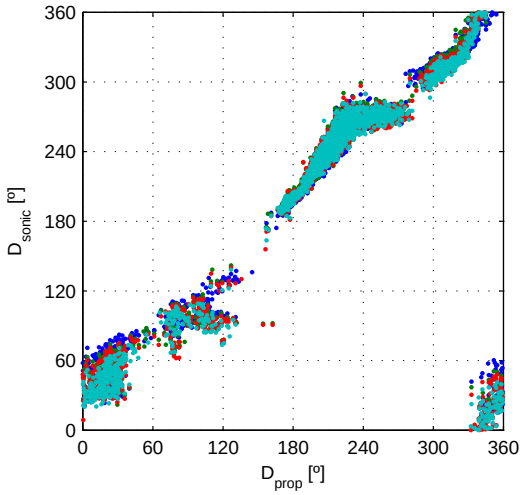


Figure 7: 10-minute mean direction of sonic anemometers vs mean direction of reference propeller.

Figure 8 represents the viaduct location and the critical wind directions according to full-scale measurements.

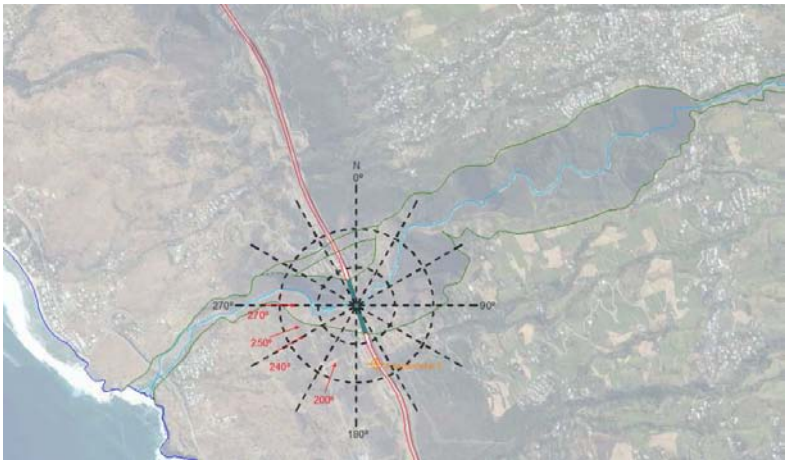

Figure 8: Scheme presenting the most critical directions observed in Grande Ravine site.

Associated with the representation in Figure 9 of the ratio $U/U_{prop}$ with the wind direction, the plot of the incidence with the mean wind direction evidences a range [20°,190°], related with the wind from the interior of the island, in which the wind has a downward direction, with maximum angle to the vertical of -1.5°. In the range [190°,20°], wind has an ascending direction characterised by two peaks: one with an average value reaching 8°, occurs for directions [215°,275°]; and the other, with an average value of 5°, occurs for directions [315°,355°].

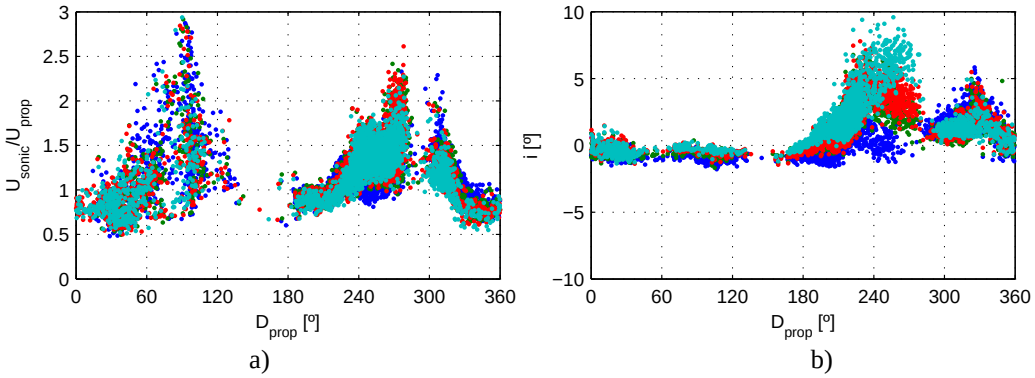


a) b)

Figure 9: Representation of (a) $U/U_{prop}$ and of (b) 10-min mean incidence with mean wind reference direction.

The gust factor, obtained from the ratio between the maximum wind velocity, calculated from a 3-s averaging period, and the mean value of velocity estimated for a 10-minute interval, is represented in Figure 10(a) as a function of the wind direction. This figure shows that the gust factor values vary in the range [1.3, 2.5]. For lower values of mean wind velocity, the average gust factor has an average value of 2, decreasing to approximately 1.5 for higher values of mean wind velocity (Figure 10b).

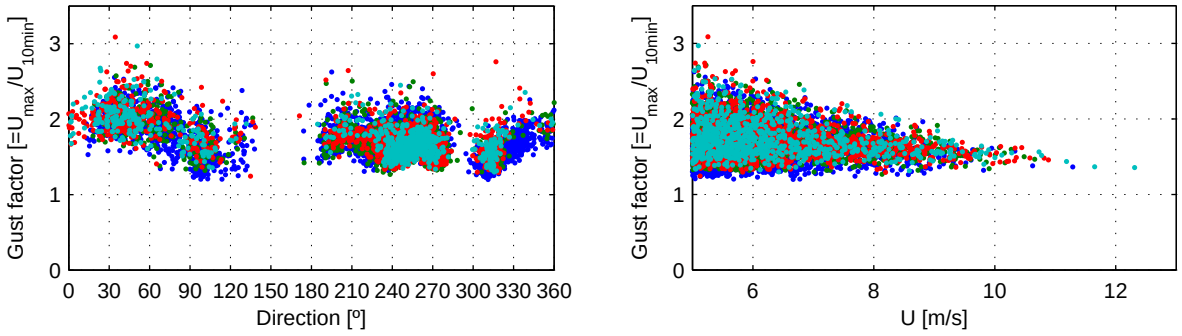


Figure 10: Gust factor variation with (a) mean wind direction and (b) mean wind velocity.

The turbulence intensity provides a measure of the variability of local turbulence, associated with each velocity component u, v and w, and is represented by the ratio between the estimate of the standard-deviation for each velocity component and the estimated mean velocity, for a 10-minute interval.

Figure 11 presents the variation of the turbulence intensity for each wind fluctuating component u, v and w with direction (a) and mean velocity (b). The average turbulence intensity of each component u, v and w of velocity tends to 0.21, 0.20 and 0.11, respectively, as the mean velocity increases. The turbulence strongly varies with the mean direction of wind. This variation is mainly due to the variation of roughness upstream the bridge site. The proximity to the walls of the ravine is evident by the strong variation of the transverse turbulence intensity.

The scales of turbulence constitute some of the parameters of highest interest in the characterisation of turbulent flows, representing the dimension of the average eddies of a turbulent flow. The turbulence length scales in longitudinal direction can be calculated directly from the integral of correlation estimates of the wind time histories or from the curve fitting of theoretical functions to the spectral estimates of wind records.

Average mean spectral estimates based on 10-minute wind turbulent component records have been obtained and are exemplified in Figure 12 for one particular wind record. Curve fitting of these data points is done using a von Karman spectral model from which parameters the longitudinal length scales $l_{[u,v,w]x}$ of u, v and w wind components are obtained.

Figure 13 presents the variation with mean wind direction and intensity of turbulence length scales of the fluctuating wind components u, v and w, obtained from spectral estimates. The analysis of this figure denotes the presence of a high level of variation with direction, which is essentially due to the upstream roughness. This variation diminishes as the mean wind velocity increases, stabilising for values around 50m, 20m e 10m in the case of u, v and w wind component, respectively. The turbulence length scale for w wind component has very low values when direction is associated with wind coming from the interior of the island (ie, in the range [40, 160]).

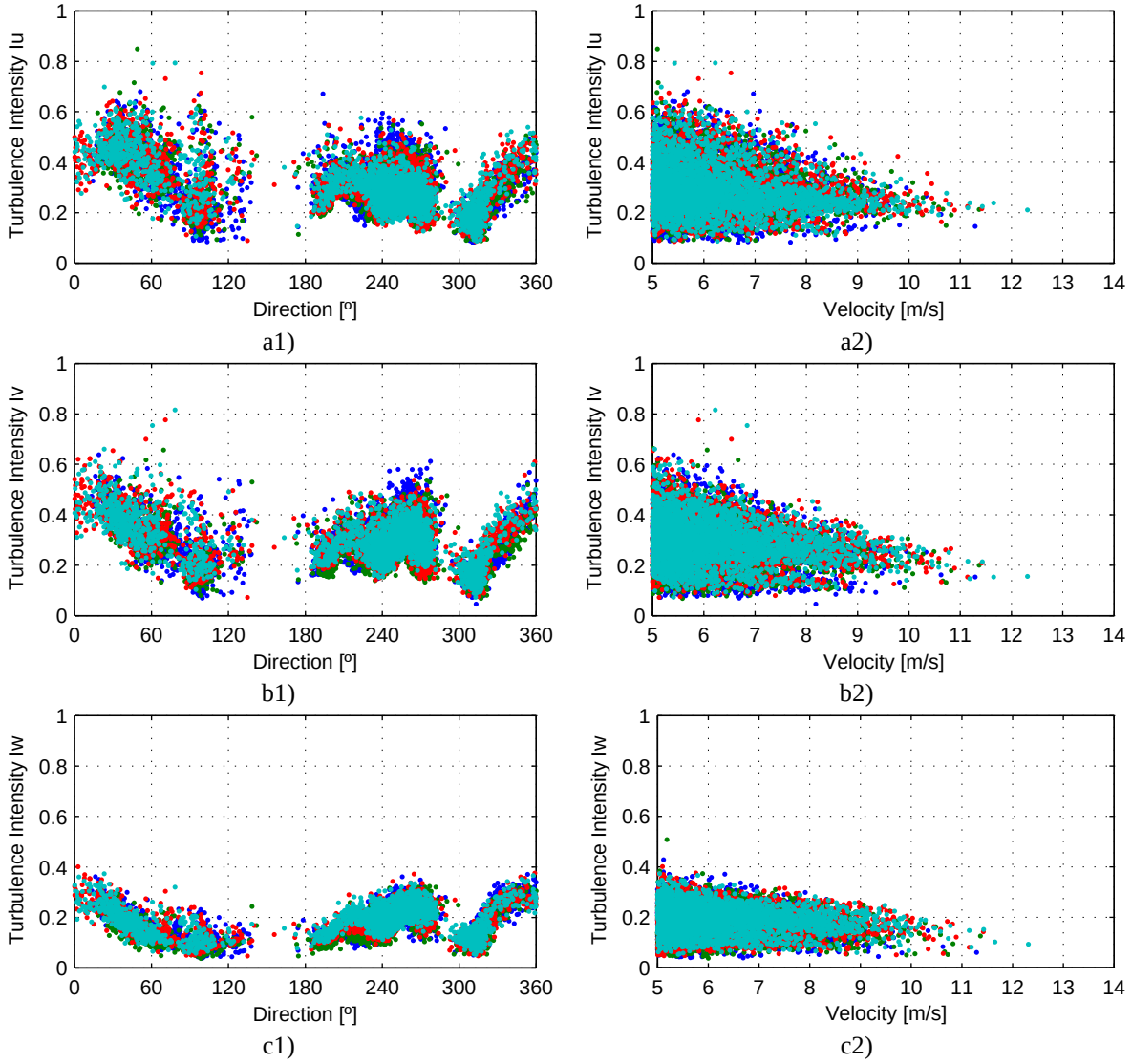


Figure 11: Turbulence intensity of wind components u, v and w variation with mean wind (a) direction and (b) velocity.

The coherence function allows the description of spatial correlation of wind turbulence in the frequency domain. This function is estimated from the ratio between the square of the modulus of the cross spectral estimates and the spectral estimates, at different points, and has been approximated, according to Davenport [5], by an exponential decay function. The fitting of experimental data by this exponential decay function provided the exponential decay coefficients presented in Figure 14, varying with mean wind direction (a) and intensity (b).

The identified exponential decay coefficients exhibit high variation with the direction, essentially due to the turbulence intensity variation for lower wind speed. From the observation of Figure 14(b), it can be concluded that exponential decay coefficients increase as the mean wind velocity grows, stabilising around 8, 4.5 and 7.5 for u, v and w wind turbulent component, respectively, ie, the coherence between wind time histories raises as the mean wind velocity increases and consequently as the turbulence intensity decreases.

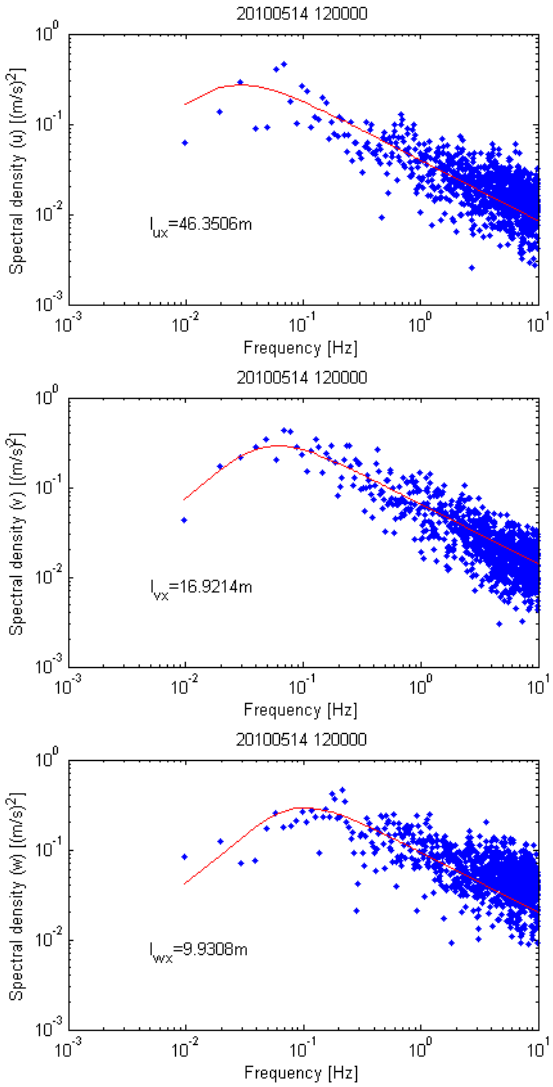


Figure 12: Fitting of von Karman curve to mean spectral estimates.

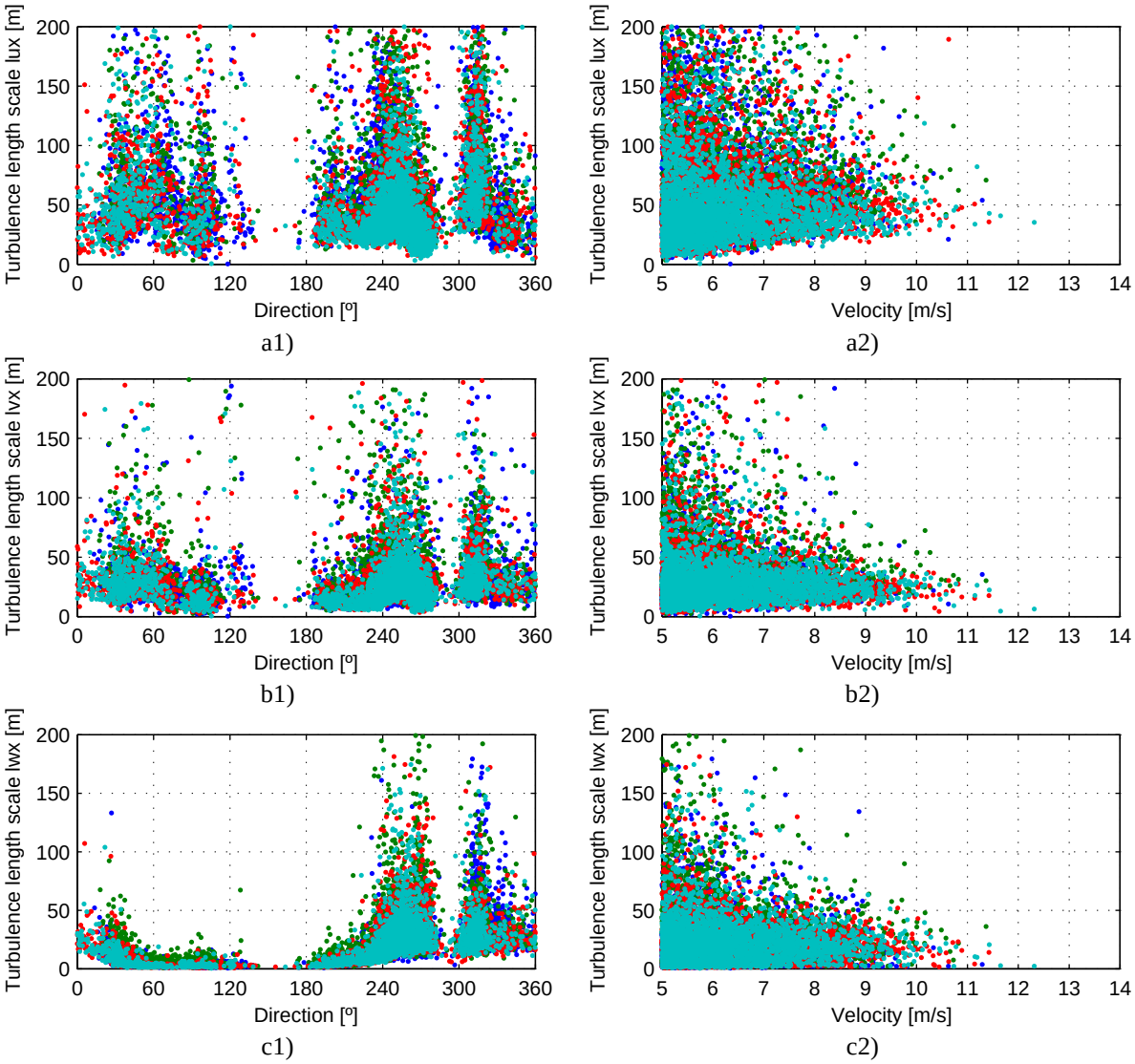


Figure 13: Variation of longitudinal turbulence length scales of wind fluctuating components u (a), v (b) and w (c), with mean wind direction (1) and intensity (2).

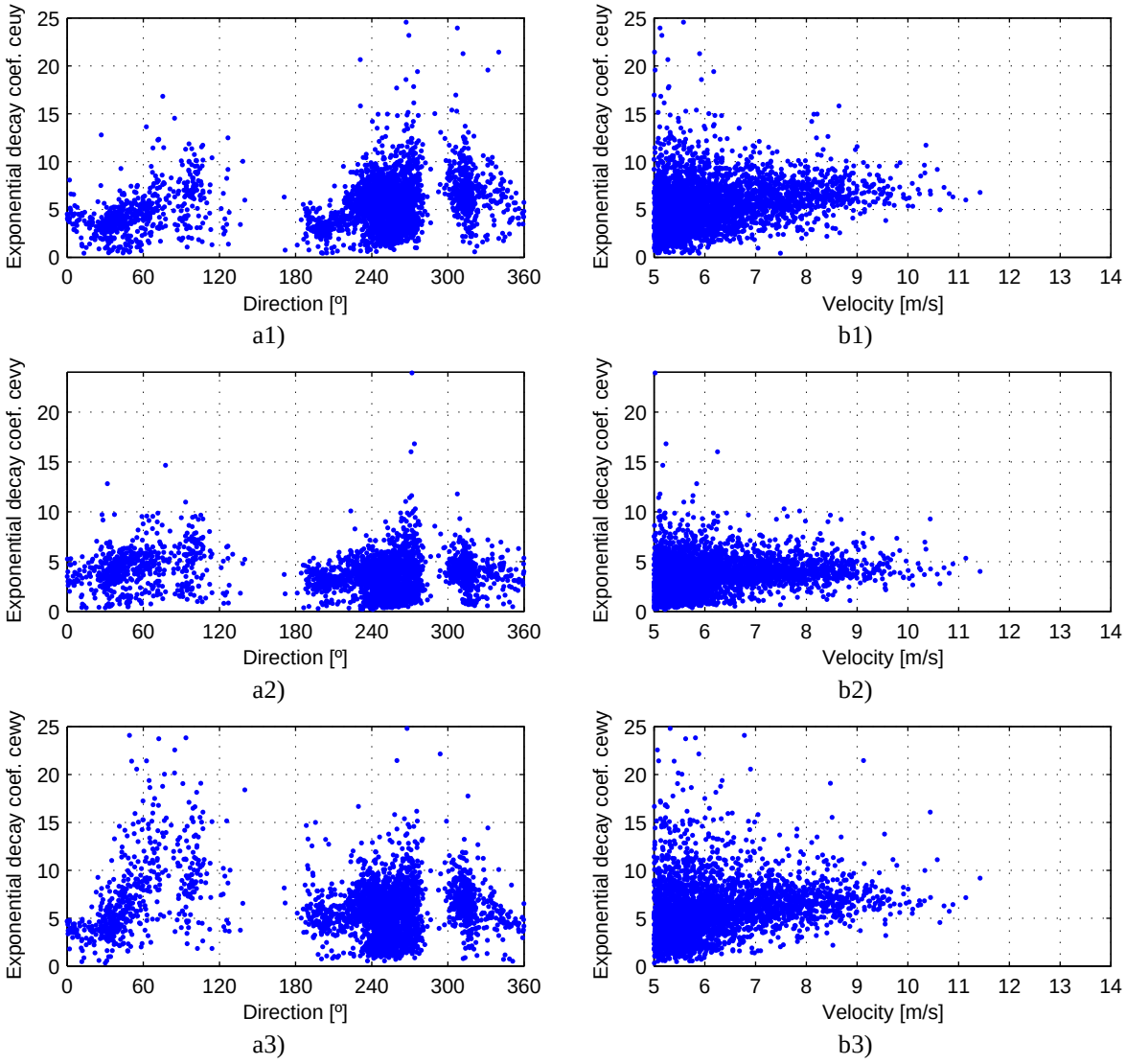


Figure 14:Variation with mean wind direction (a) and intensity (b) of exponential decay coefficients of wind turbulent component u, v and w.

## 4 WIND MODEL

Based on the results from full-scale measurements during the 2-year monitoring period above described, a wind model for the Grande Ravine site is proposed in this section, and a comparison is made with parameters defined at design stage on the basis of numerical CFD and wind tunnel studies.

### 4.1 Critical wind directions

The analysis of collected wind records with mean wind velocity greater than 7.5m/s allowed the identification of the prevalent wind directions. According to the representation of Figure 15(a), it can be concluded that the most common directions are in the range [200°, 360°], corresponding to wind perpendicular to the viaduct axis. Moreover, it could be observed that the ravine causes a “bottleneck” effect (see Figure 7).

Figure 15(b) represents the coefficients defined by the ratio between the mean wind velocity collected at the bridge site (anemometers 1 to 4) and the mean wind velocity measured by

the anemometer located outside the bridge (propeller anemometer no. 5). For the prevailing wind direction, the ratio $U/U_{prop}$ varies in the range [0.9, 1.8].

Table 1 presents the qualitative representation of the results obtained from Figure 15(a) and the average value of $U/U_{prop}$ ratio estimated from Figure 15(b) with angular amplitude of 15° (±7.5°). The analysis of Figure 15 and of this table evidences that the direction 250°, normal to the viaduct axis, presents the highest occurrence and the highest intensity winds, therefore being selected as the most critical in the present study. Furthermore, Figure 15 shows that above 280° the wind presents low occurrence and intensity. Based on this information, the following directions were taken as critical for analysis: 200°, 240°, 240° and 270°. These are indicated in Figure 8.

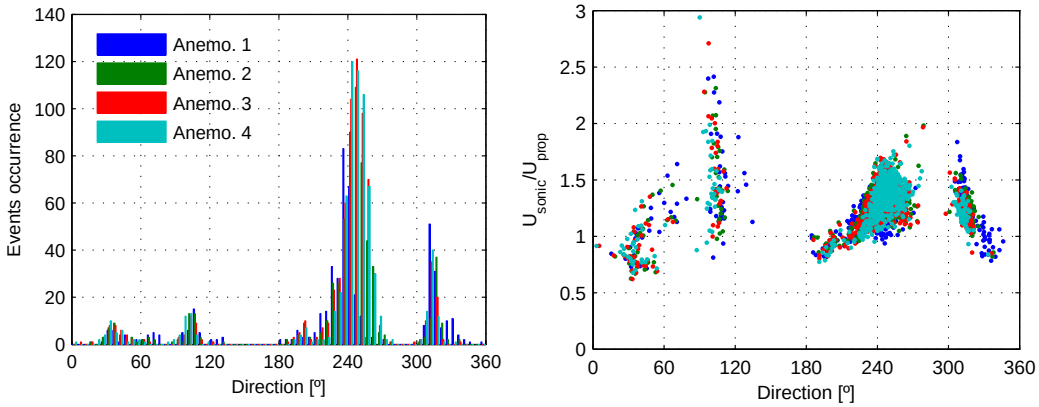


(a) (b)

Figure 15: (a) Mean wind prevalence and (b) $U_{sonic}/U_{prop}$ variation with wind direction.

| Directions | Angle with normal to deck | Full-scale measurements | |
|---|---|---|---|
| | | Prev. direction | $U/U_{prop}$ |
| 200° | -50° | ++ | 1.05 |
| 240° | -10° | +++ | 1.44 |
| 250° | 0° | +++ | 1.59 |
| 270° | 20° | ++ | 1.55 |
| 300° | 50° | + | 1.32 |
| 360° | 110° | + | 0.98 |

Table 1: Wind parameters for most prevalent directions.

## 4.2 Wind velocity

In the design study [7], the reference velocity of 34m/s was considered, according to the proposal by Eurocode 1 [8] for the Reunion Island territory. This velocity represents a mean wind velocity at 10m height on a flat field terrain type associated with a 50-year return period.

To assess the mean wind velocity at the Grande Ravine site for a 50-year return period on the basis of full-scale measurements, the reference velocity is affected by the roughness coefficient obtained from meteorological data [7] and by transfer coefficients calculated by averaging the values of the ratio between the 10-minute mean velocity measured by sonic anemometers at the viaduct and the 10-minute mean velocity measured, synchronously, by the propeller anemometer positioned at 10m height.

Table 2 summarises the obtained mean wind velocity values for the most critical directions, together with the values adopted in design [7]. It can be observed that the mean wind velocity derived from full-scale measurements is generally smaller than the one adopted in design.

This difference is even more relevant for the direction 200°, meaning that the effect of the ravine is not felt in this direction.

| Directions | Full-scale [m/s] | Adopted in design [m/s] |
|---|---|---|
| 200° | 30.64 | 49.7 |
| 240° | 42.24 | 51.13 |
| 250° | 46.48 | - |
| 270° | 45.46 | 56.5 |

Table 2: Mean wind design velocity definition for most critical directions: full-scale measurements and adopted design model.

### 4.3 Wind incidence

Table 3 presents the comparison between mean incidences registered for the most penalising directions and the ones adopted in design. Significant differences with regard to the design hypotheses are found, fact that may be explained by the very complex topography of the bridge site. In effect, the abrupt walls of the ravine and the presence of a small hill reflect the influence of upstream topography and roughness in the flow at the measuring site. Full-scale incidence values exhibit always positive value (ascending direction), growing as the direction moves from 200 to 270°.

| Direction | Full-scale | Adopted in design |
|---|---|---|
| 200° | 0.02 | 6.00 |
| 240° | 0.76 | 0.00 |
| 250° | 1.61 | - |
| 270° | 3.54 | 6.00 |

Table 3: Mean wind incidence for most penalising directions: full-scale measurements and adopted in design.

### 4.4 Turbulence intensity

Table 4 presents the comparison, for the most penalising directions, of turbulence intensity of the wind fluctuating components u, v and w, obtained from full-scale measurements with the values adopted in design. The analysis of this table shows that the values obtained from full-scale measurements are higher than the design values. The values of lateral and vertical turbulence intensity tend to grow for directions in the range [240°, 270°] due to the influence of the walls of the ravine upstream the viaduct site.

| Turbulence intensity | Direction | 200° | 240° | 250° | 270° |
|---|---|---|---|---|---|
| Iu | Full-scale | 0.2597 | 0.2336 | 0.2497 | 0.2481 |
| | Adopted in design | 0.1690 | 0.0931 | - | 0.0920 |
| Iv | Full-scale | 0.2317 | 0.2331 | 0.2605 | 0.2993 |
| | Adopted in design | 0.1352 | 0.1117 | - | 0.1012 |
| Iw | Full-scale | 0.1147 | 0.1454 | 0.2134 | 0.2395 |
| | Adopted in design | 0.1183 | 0.0465 | - | 0.0460 |

Table 4: Turbulence intensity for most penalising directions: full-scale measurements and adopted in design.

The influence of the local roughness in the fluctuating wind components is also notorious. For a wind direction of 200°, the turbulence intensity ratios Iv/Iu and Iw/Iu, presented in Table 5, are 0.892 and 0.442, respectively. Although turbulence conditions are higher, these ratios are comparable to the ratios presented in [10, 11] for flat surrounding conditions,

confirming that for this direction the effect of the ravine is not significantly felt. When the wind direction tends to 270°, the effect of the ravine topography and wall roughness on wind turbulence components tend to increase, reaching for this particular direction of 270° almost equal turbulence intensities in the three wind components (see Table 5).

| Direction | Full-scale | | Adopted in design | |
|---|---|---|---|---|
| | Iv/lu | lw/lu | lv/lu | lw/lu |
| 200° | 0.892 | 0.442 | 0.800 | 0.700 |
| 240° | 0.998 | 0.622 | 1.200 | 0.500 |
| 250° | 1.043 | 0.855 | - | - |
| 270° | 1.166 | 0.965 | 1.100 | 0.500 |

Table 5: Ratios lv/lu and lw/lu: full-scale measurements and adopted in design.

## 4.5 Gust factor

Table 6 presents the mean gust factor for the most penalising directions obtained from the full-scale measurements, as well as the values adopted in design. It is shown that the gust factors obtained from full-scale measurements are higher than the design values and are coherent with the values registered for the turbulence intensity presented in Table 4.

| Direction | Full-scale | Adopted in design |
|---|---|---|
| 200° | 1.67 | 1.48 |
| 240° | 1.59 | 1.26 |
| 250° | 1.61 | - |
| 270° | 1.64 | 1.26 |

Table 6: Gust factor for most penalising directions: full-scale measurements and adopted in design.

## 4.6 Turbulence length scales

Turbulence length scales for the most penalising directions obtained from full-scale measurements are summarised in Table 7 and the ratios to the longitudinal turbulence length scales presented in Table 8. The analysis of these tables shows that the turbulence length scale ratios associated with the wind direction 200° are coherent with the ones shown in the extensive review made in [11] and also similar to the ratios presented in [12]. As the direction increases from 240° to 270°, the longitudinal length scale tends to slightly decrease and the lateral and vertical ratios tend to increase.

| Turbulence length scales | 200° | 240° | 250° | 270° |
|---|---|---|---|---|
| lux | 50.14 | 44.42 | 47.92 | 40.11 |
| lvx | 15.39 | 19.44 | 21.41 | 17.15 |
| lwx | 3.97 | 10.87 | 15.93 | 16.61 |

Table 7: Turbulence length scales for most penalising direction.

| Direction | Full-scale | | Adopted in design | |
|---|---|---|---|---|
| | lvx/lux | lwx/lux | lvx/lux | lwx/lux |
| 200° | 0.307 | 0.079 | 0.300 | 0.250 |
| 240° | 0.438 | 0.245 | 0.200 | 0.250 |
| 250° | 0.447 | 0.332 | - | - |
| 270° | 0.428 | 0.414 | 0.150 | 0.125 |

Table 8: Ratio between turbulence length scales of lateral and vertical wind component and turbulence scale of longitudinal wind component: full-scale measurements and adopted in design.

Table 9 shows the turbulence length scales measured for the transversal direction (y direction) for the most penalising directions. Table 10 presents the values registered from full-scale measurements of the relations between turbulence length scales, together with the reference values based on the theory of homogeneous and isotropic turbulence [13]. It can be concluded that the values from full-scale measurements tend to be similar to the literature values as the wind direction tends to 270°. The values registered for wind direction 200° illustrate the elongated character of the eddies within the flow.

| Transversal length scale | 200° | 240° | 250° | 270° |
|---|---|---|---|---|
| Luy | 120.80 | 50.96 | 54.09 | 43.67 |
| Lvy | 77.45 | 65.37 | 61.08 | 42.75 |
| Lwy | 29.98 | 35.78 | 40.36 | 33.01 |

Table 9: Transversal length scale for most penalising directions.

| | Lux/Lvy | Luy/Lux | Lvx/Lvy | Lwy/Lwx |
|---|---|---|---|---|
| Theory [13] | 1 | 0.5 | 0.5 | 1 |
| 200° | 0.757 | 2.060 | 0.434 | 4.114 |
| 240° | 0.823 | 0.947 | 0.444 | 2.144 |
| 250° | 0.926 | 0.956 | 0.537 | 1.837 |
| 270° | 1.010 | 1.011 | 0.726 | 1.086 |

Table 10: Ratio between turbulence length scales of wind turbulence component u, v and w, in longitudinal and transversal directions.

## 4.7 Coherence coefficients

Table 11 systematises the coherence coefficients for the most conditioning directions obtained from full-scale measurements.

The data presented in Figure 11 demonstrate that when the wind velocity increases, the turbulence intensity tends to stabilise around a value which corresponds to the stationary pattern of atmospheric conditions. The same trend is observed for the coherence coefficients. However, the dispersion of coherence coefficients is lower, starting from a lower value at low wind velocity and increasing till stabilisation for higher wind velocity. As a consequence, the values of the coherence coefficients for each direction were obtained by adjusting a curve, to the higher values of wind velocity in the limit of the coherence coefficients registered values.

| Coherence coefficients | 200° | 240° | 250° | 270° |
|---|---|---|---|---|
| ceuy | 4.75 | 8.27 | 9.45 | 8.19 |
| cevy | 4.23 | 5.25 | 6.19 | 7.84 |
| cewy | 6.28 | 8.23 | 8.72 | 7.77 |

Table 11: Coherence coefficients for most penalising directions.

## 4.8 Wind model from full-scale measurements

Table 12 summarises the Grande Ravine wind model extracted on the basis of the full-scale measurements systematised in the previous sections. Comparing the proposed wind model with the one adopted in design, it can be concluded that the mean wind component of full-scale wind model is less severe, while turbulence intensities are much higher and turbulence length scales much lower and with dimensions close to the viaduct dimensions. The transversal length scales and coherence coefficients are similar to the values adopted in design.

| Direction [°] | 200 | 240 | 250 | 270 |
|---|---|---|---|---|
| Mean wind velocity [m/s] | 30.64 | 42.24 | 46.48 | 45.46 |
| Incidence [°] | 0.02 | 0.76 | 1.41 | 3.54 |
| Turbulence Intensity | | | | |
| u | 0.2597 | 0.2336 | 0.2497 | 0.2481 |
| v | 0.2317 | 0.2331 | 0.2605 | 0.2993 |
| w | 0.1147 | 0.1454 | 0.2134 | 0.2395 |
| Turbulence length scales [m] | | | | |
| lux | 50.14 | 44.42 | 47.92 | 40.11 |
| lvx | 15.39 | 19.44 | 21.41 | 17.15 |
| lwx | 3.97 | 10.87 | 15.93 | 16.61 |
| Luy | 120.80 | 50.96 | 54.09 | 43.67 |
| Lvy | 77.45 | 65.37 | 61.08 | 42.75 |
| Lwy | 29.98 | 35.78 | 40.36 | 33.01 |
| Coherence coefficients | | | | |
| ceuy | 4.75 | 8.27 | 9.45 | 8.19 |
| cevy | 4.23 | 5.25 | 6.19 | 7.84 |
| cewy | 6.28 | 8.23 | 8.72 | 7.77 |

Table 12: Grande Ravine wind model based on full-scale measurements.

## 5 CONCLUSIONS

This paper presents a comprehensive study of the wind characteristics at the Grande Ravine viaduct site, crossing a deep ravine. The research is based on the analysis of wind collected by means of a monitoring system installed in the structure over a 2-year period.

The parameters extracted from the treatment of the data recorded by the four sonic anemometers located along the bridge deck and the propeller anemometer placed 250m outside the viaduct were compared with those defined in the context of the viaduct design, based on a CFD numerical study and on wind tunnel test.

Based on the full-scale measurements, a wind model is proposed, whose parameters have been summarised in Table 12. The comparison between this model and the one adopted in design evidences that the mean wind component of the full-scale wind model is less severe than the one adopted in design, while turbulence intensities are much higher. These characteristics are not necessarily conservative, as they can lead to higher structural dynamic response. This wind model will now be used to validate the calculations conducted at design stage.

## ACKNOWLEDGEMENTS

The present work has been developed in the sequence of a collaboration established between the University of Porto and the design office SETEC.tpi, responsible for the design and installation of the monitoring system at the viaduct site. Additional cooperation has been established with CSTB. The first author acknowledges the PhD scholarship (SFRH/BD/46126/2008) funded by FCT.

## REFERENCES

[1] Croiset J-E, Ryckaert J, Spielmann A, Viel G. 2005. *Le viaduc de la Grande Ravine: Un pont à effet d'arc limité et contrôlé*. Travaux, No.823:110-6.

[2] Viel, G., Boileau, C., Ryckaert, J. 2008. *Viaduc de la Grande Ravine, Tranche conditionnelle 1 : Instrumentation en service de l'ouvrage*. Report 18353/S/T/E2051, SETEC.

[3] Callewaert F, Laurent E. 2009. *La Grande Ravine. Manuel d'utilisation du logiciel*. Paris: ADVITAM; 2009.

[4] Bastos, F., Caetano, E., Cunha, A., Cespedes, X. and Flamand, O. 2000. *Characterisation of the wind properties in the Grande Ravine Viaduct*. Paper submitted to Engineering Structures.

[5] Simiu E, Scanlan RH. 1996. *Wind Effects on Structures: Fundamental and Applications to Design*. Third Edition ed: John Wiley & Sons.

[6] Barré C. *EN-CAPE 02.141 C-V0 - Caractérisation du vent sur 4 sites de la route des Tamarins à la Réunion - Étude en soufflerie atmosphérique sur maquettes topographiques.* Nantes: CSTB; 2002.

[7] Delaunay D, Sabre M. *EN-CAPE 02.109 C-V1 - Calcul numérique du vent sur quatre sites de la route des Tamarins à la Réunion*. Nantes: CSTB; 2002.

[8] Delaunay D. *EN-AEC 99.1 - Chartographie des vents cyclonics dans les departments d'Outre mer*. Nantes: CSTB; 1999.

[9] ENV1991-2-4. *Eurocode 1: Basis of design and actions on structures - Part 2-4: Actions on structures - Wind actions*. Brussels, Belgium ed: Comité Europeen de Normalisation; 1995.

[10] Hui MCH, Larsen A, Xiang HF. Wind turbulence characteristics study at the Stonecutters Bridge site: Part I - Mean wind and turbulence intensities. Journal of Wind Engineering and Industrial Aerodynamics. 2009;97:22-36.

[11] Solari G, Piccardo G. Probabilistic 3-D turbulence modeling for gust buffeting of structures. Probabilistic Engineering Mechanics. 2001;16:73-86.

[12] Cremona C, Foucriat J-C. Comportement au vent des ponts. Paris - France: Presses de l'école nationale des Ponts et Chaussées; 2002.

[13] Baloche C, Barnaud G, Bietry J, Chevalier J-L, Delaunay D, Duforestel T et al. Traité de Physique du Batiment - Tome 1 : Connaissances de base. Paris, France: Centre Scientifique et Technique du Bâtiment (CSTB); 1995.